Contrasting mechanical behavior in precipitation hardenable $Al_XCoCrFeNi$ high entropy alloy microstructures: single phase *FCC* vs. dual phase *FCC-BCC*

Sindhura Gangireddy[a*], *Bharat Gwalani[b*], Rajarshi Banerjee[b], Rajiv S. Mishra[a]

[a]*Advanced Materials and Manufacturing Processes Institute, University of North Texas, Denton, TX 76207*

[b]*Materials Science and Engineering, University of North Texas, Denton, TX 76207*

Corresponding author: *bharatgwalani@my.unt.edu*
*Equal contributing authors

Abstract:
$Al_xCoCrFeNi$ is a prominent high entropy alloy system with varying crystal structure from *FCC* to *BCC* depending on aluminum content. The mechanical behavior of $Al_{0.7}CoCrFeNi$ with dual phase *FCC+BCC* microstructure has been compared with that of single phase *FCC* $Al_{0.3}CoCrFeNi$. Both quasi-static and dynamic strain rate regimes were investigated. Hypo-eutectic $Al_{0.7}CoCrFeNi$ showed much higher strength due to fine lamellar microstructure with a large number of *FCC-BCC* interphase boundaries. But this also lead to lower strain rate sensitivity due to the long range nature of these interfaces, overcoming them is indifferent with temperature elevation to assist slip, thus making them athermal barriers. Both these precipitation hardenable alloys were aged to induce precipitation of ordered $L1_2$ in the *FCC* phase. This coherent nano-scale $L1_2$ precipitate caused a significant increase in the yield strength of both single phase and dual phase structures, while reducing the strain rate sensitivity (SRS) only slightly. $L1_2$ precipitation in *FCC* matrix greatly enhanced twinning during dynamic deformation. Large-scale deformation twins were observed in coarse $Al_{0.3}CoCrFeNi$ *FCC* and *FCC+*$L1_2$ microstructures. The scale of deformation twins were much smaller in the dual phase $Al_{0.7}CoCrFeNi$ whose refined lamellae width retarded twinning. The lamellar structures, nevertheless, had higher work hardening due to their higher dislocation density storage capability.

Keywords: strain rate sensitivity; work hardening; deformation twinning; dual phase vs. single phase high entropy alloy; $Al_XCoCrFeNi$; precipitation effect.

Introduction:

High-entropy alloys (HEAs) are a new paradigm-shift in metallic alloy development consisting multiple principal elements. Significant multi-element effects as compared with conventional alloys have been proposed and investigated in HEAs, including high entropy, sluggish diffusion, lattice distortion, and cocktail effects [1-4]. They offer extraordinary tunability in microstructural design [5-6] for enhanced strength, along with good ductility from simple crystal structures. $Al_xCoCrFeNi$ is prominent among several alloy systems identified on this alloy-design strategy. It changes from *FCC* to *BCC* structure with increasing aluminum content, x = 0 to 2, and displays a wide spectrum of mechanical behavior [7-9]. At intermediate aluminum levels ~ x = 0.6-0.9, the alloy is near eutectic and forms lamellar microstructures composed of both *FCC* and *BCC* phases, through which a balance of high fracture strength and ductility could be achieved

[10]. However, there have not been any studies on how this dual phase microstructure affects critical mechanical properties such as strain rate sensitivity (a measure of increment in strength of the material at elevated strain rates) and work hardening rate (the increment in stress required to deform the material at further plastic strains), both of which determine failure resistance of the material [11].

It has been recently proposed that *FCC* based HEAs offered outstanding strain rate sensitivities (SRS) compared to conventional *FCC* alloys [12, 13]. SRS values reaching m ~ 0.06 level have been reported in single phase *FCC* $Al_{0.3}$CoCrFeNi [14], which usually only occur in nano-crystalline materials. Significant strength contributions arise from internal stresses in HEAs which have large friction stress from heavy lattice distortion and varying dislocation mobility [15], along with strong solid solution strengthening [16]. These short-range obstacles to dislocation motion can be thermally overcome (with temperature increase) and therefore have temperature/strain rate dependence, leading to elevated SRS values. Stacking fault energy (SFE) is expected to be very low in Al_xCoCrFeNi system, < 30 mJ/mm^2 [17]. Low SFE is expected to hinder dynamic recovery enhancing dislocation storage capacity/promoting deformation twinning, leading to overall higher work hardening rates [12, 13].

In this study, we compare mechanical behavior of dual phase near-eutectic $Al_{0.7}$CoCrFeNi microstructures with that of single phase $Al_{0.3}$CoCrFeNi microstructures and contrast the differences in their strain rate sensitivities and work hardening rates. Both $Al_{0.3}$CoCrFeNi and $Al_{0.7}$CoCrFeNi are precipitation hardenable and annealing treatments could be used to further strengthen the alloys. The effect of introducing precipitates in each of these two types of microstructures is investigated through aging at moderately high temperatures.

Experimental Procedure:

The thermomechanical processing treatment steps for attaining the desired microstructures are charted in Figure 1. Both the alloys were prepared by conventional arc melting. They were first homogenized at high temperature for softening the alloy by annihilating dislocations and micro-segregations formed during casting. This was followed by room temperature cold rolling to desired thickness reductions (50% in $Al_{0.3}$CoCrFeNi, and 30% in $Al_{0.7}$CoCrFeNi). The rolled materials were yet again annealed at high temperature to recrystallize and further homogenize the microstructure. These conditions are termed 0.3HM and 0.7HM for $Al_{0.3}$CoCrFeNi and $Al_{0.7}$CoCrFeNi respectively. The homogenized conditions are subsequently aged again at moderate temperature to introduce precipitation of $L1_2$ intermetallic phase. These conditions were called 0.3HM-550 and 0.7HM-580 respectively. In all the heating steps, the samples were placed in the furnace after set temperature was reached and cooled by water quenching after specified treatment time to eliminate microstructural evolution during the ramps. These microstructures were studied using scanning and transmission electron microscopes (SEM, TEM), and electron back-scatter diffraction (EBSD). Samples were subjected to mechanical testing procedures: quasi-static tensile testing at 10^{-3} s^{-1}, and dynamic deformation using split-Hopksinson pressure bar (SHPB) at 10^3 s^{-1} initial strain rates [18]. We performed at least three high and low strain rate tests on each condition and observed very good repeatability.

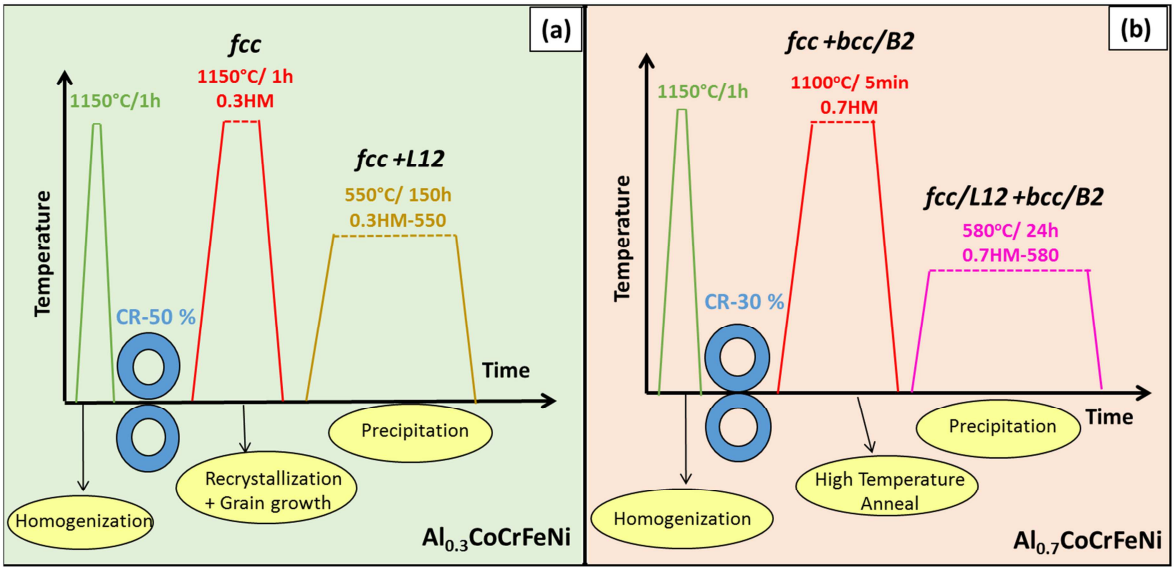

Figure 1: *Thermomechanical processing steps applied on (a) $Al_{0.3}$CoCrFeNi to obtain single phase FCC and FCC+$L1_2$, and (b) $Al_{0.7}$CoCrFeNi for obtaining dual phase FCC+BCC/B2 and FCC/$L1_2$+BCC/B2 microstructures.*

Results and Discussion:

Microstructures

The single phase microstructures resulting from $Al_{0.3}$CoCrFeNi processing are summarized in Figure 2. The images on the top are low magnification EBSD scans capturing the overall microstructure, while those below are TEM micrographs showing high magnification images along with selected area diffraction patterns (SADP) detailing phase distribution. Figure 2(a and b) depicts the solutionized alloy (0.3HM) from CR50% + 1150°C/1h, which was single phase *FCC* with coarse grains of ~150 µm. The bright field TEM (BFTEM) image is shown in Figure 2 (b), along with the SADP from [110] and [1-1-2] *FCC* zone axis (ZA) as the inset showed only the fundamental *FCC* reflections. Subsequent annealing at 550°C/150h (0.3HM-550) formed nano-scale $L1_2$ precipitates, as seen from Figure 2(c and d). This sample exhibited additional super lattice reflections at {001} and {011} positions in the [110] *FCC* diffraction pattern (inset Figure 2 (d)). The corresponding dark field (DF) image recorded from the super-lattice spot marked with a circle in the SADP pattern clearly revealed the ordered $L1_2$ precipitates of spherical form, with size ranging from 3 to 10 nm.

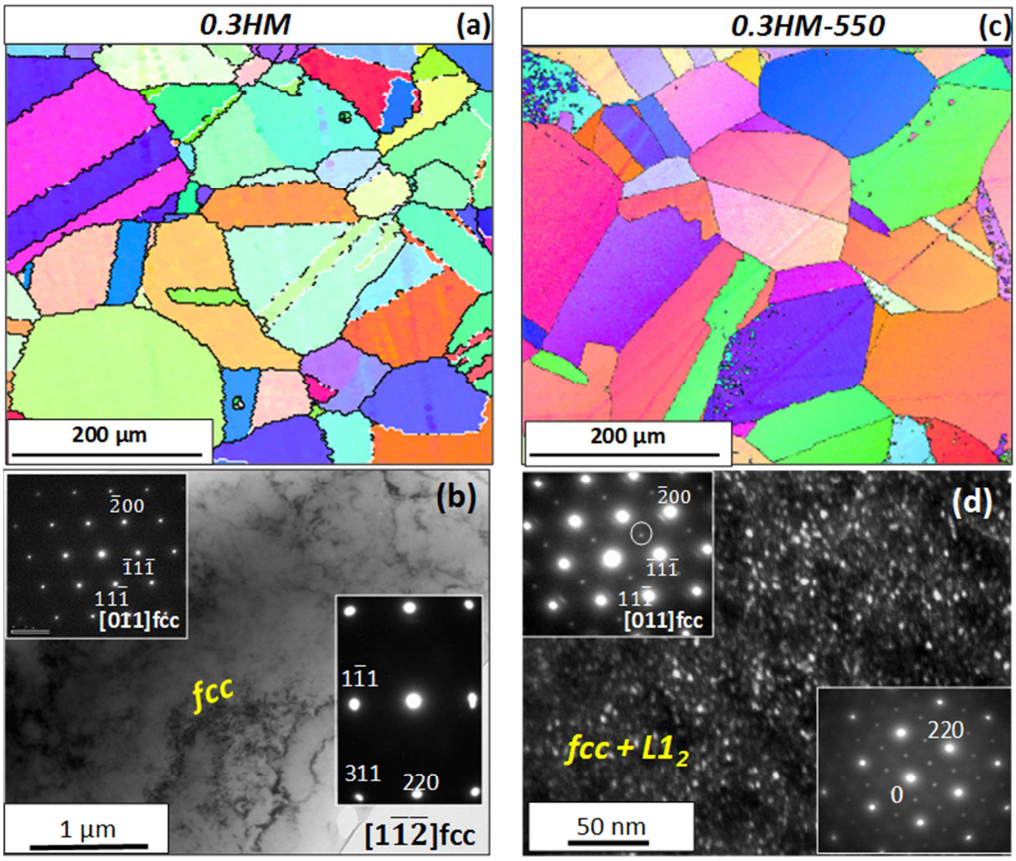

Figure 2. *Microstructures from thermomechanical processing of $Al_{0.3}$CoCrFeNi with IPF images from EBSD on top, and TEM images with SADP diffraction patterns below: (a) EBSD (b) TEM results of solutionized microstructure from CR50% + 1150°C/1h (0.3HM) showing coarse single phase FCC grains, and (c) EBSD (d) TEM results aged microstructure from CR50% + 1150°C/1h + 550°C/150h (0.3HM-550) showing precipitation of nano-scale $L1_2$ highlighted from additional super-lattice reflections.*

Figure 3 demonstrates the two dual phase microstructures from thermomechanical processing of $Al_{0.7}$CoCrFeNi alloy. Figure 3(a and b) summarizes the solutionized condition (0.7HM) from CR30% + 1100°C/5min showing a lamellar microstructure in EBSD, along with a phase map in inset highlighting the altering *FCC-BCC* phases. The thicknesses of the lamellar and interlamellar phases were very fine ~1-2 µm. TEM examination was done from either region, revealing that *FCC* phase is disordered *FCC* whereas the *BCC* phase consisted of a ordering of the lattice structure. BF-TEM image below shows the presence of a hypo-eutectic structure where *FCC* appears to be the primary phase [19]. The SADP from *FCC* (zone axis = $[011]_{FCC}$) and *BCC* (zone axis = $[001]_{BCC}$) are shown as insets. The presence of extra super lattice spot at {001} position in in $[001]_{BCC}$ zone axis clearly suggests ordering of *BCC* lattice in this region. Scanning TEM (STEM)-Energy Dispersive Spectroscopy EDS compositional mapping at higher magnification showed compositional segregation within the *BCC* phase (as clearly seen in the Cr map in inset) inferring presence of both *BCC* and B2 phases (inset Figure 3 (b)). Similar characterization was performed on the 0.7HM-580 aged condition (refer Figure 3 (c and d)). At

low magnification level in EBSD, it resembled the 0.7HM condition with a fine-lamellar alternating *FCC-BCC* near-eutectic microstructure. But at high magnification in TEM, the SAD pattern from $[011]_{FCC}$ zone axis shows the presence of the extra {001} super-lattice spot in this condition, clearly depicting ordering of *FCC* phase as well, which is different from 0.7HM. A compositional partitioning within *FCC*, as seen from inset of Al map from STEM-EDS (inset of Figure 3(d)), further established presence of *FCC*+$L1_2$ (ordered *FCC*) phase. The size and distribution of $L1_2$ precipitates in the *FCC* region here are very identical to those in the single phase 0.3HM-550 condition. The *BCC* region was similar to solutionized condition 0.7HM where presence of *BCC*+B2 could be deduced.

Eutectic microstructures are often characterized by elemental segregation into the second phase. Figure 3(e) summarizes elemental partitioning between *FCC* and *BCC* phases captured using STEM-EDS mapping. A 1-D compositional line profile along the highlighted white arrow showed severe depletion of Al and Ni from *FCC r*egions. The second *BCC-type phase* is hence rich in Al and Ni and therefore has a strong tendency to form the Al-Ni intermetallic B2. Furthermore, the B2 phase undergoes a phase separation to form Cr rich *BCC* precipitates within itself at low temperature, probably by spinodal decomposition [20].

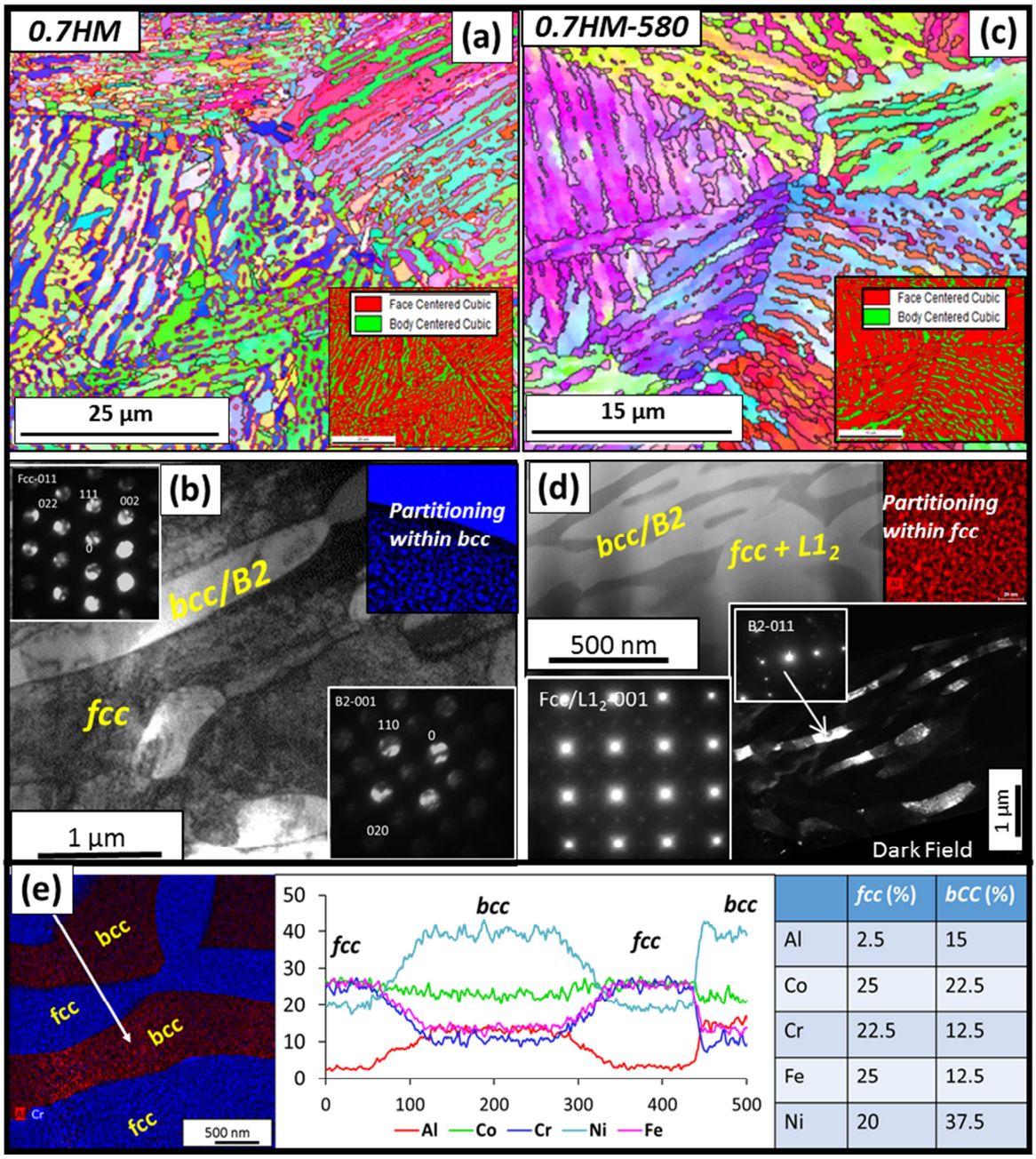

	fcc (%)	bCC (%)
Al	2.5	15
Co	25	22.5
Cr	22.5	12.5
Fe	25	12.5
Ni	20	37.5

Figure 3. *Microstructures from thermomechanical processing of $Al_{0.7}$CoCrFeNi: (a and b) solutionized alloy 0.7HM (CR 30% + 1100°C/5min), (c and d) aged condition 0.7HM-580 (CR50% + 1100°C/5min + 580°C/24h). Both IPF images from EBSD with phase map insets show lamellar near-eutectic microstructures. TEM images show 0.7HM has disordered FCC phase while BCC+B2 both are present. Post aging, 0.7HM-580 ordered $L1_2$ precipitates in FCC. (c) STEM-EDS of 0.7HM showing elemental segregation between the FCC-BCC phases. The FCC phase is depleted in Al and compositionally ~ $Al_{0.1}$CoCrFeNi, while the BCC phase is rich in Ni and Al.*

Mechanical Behavior

Mechanical testing was conducted on the above four microstructures at two drastically different strain rates. A computer-controlled mini-tensile testing machine was used for quasi-static deformation at an initial strain-rate of 10^{-3} s^{-1}. Dynamic compression was performed using a split-Hopkinson pressure bar (SHPB) system [18] at a strain rate of 2×10^{3} s^{-1}. True stress-strain curves from the two regimes are displayed in Figure 4.

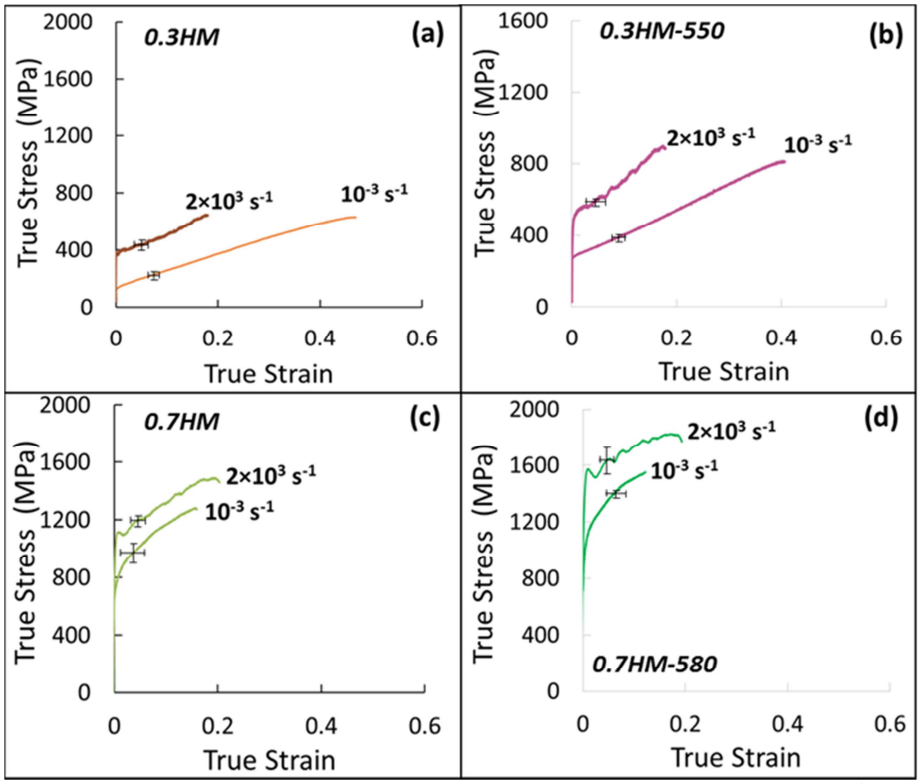

Figure 4: *Stress-strain plots from standard quasi-static tensile testing at 10^{-3} s^{-1} and dynamic deformation using split-Hopkinson pressure bar at 2×10^{3} s^{-1} strain rate: (a) solutionized $Al_{0.3}$CoCrFeNi 0.3HM (single phase FCC), (b) $Al_{0.3}$CoCrFeNi aged 0.3HM-550 (FCC+$L1_2$), (c) $Al_{0.7}$CoCrFeNi solutionized 0.7HM (FCC + BCC/B2), and (d) aged $Al_{0.7}$CoCrFeNi 0.7HM-580 (FCC/$L1_2$ + BCC/B2).*

The quasi-static yield strength of the pure *FCC* microstructure (0.3HM) was low ~160 MPa with high ductility of ~64%, comparable to earlier reports on tensile strength of coarse-grained $Al_{0.3}$CoCrFeNi [3, 21]. Upon aging, 0.3HM-550 showed higher strength of ~250 MPa and this 48% increase is attributed to precipitate strengthening from the intermetallic $L1_2$ phase [3, 21]. Due to the coherent nature of these precipitates, ductility remained high at ~56%. The dual phase *FCC-BCC* microstructures of $Al_{0.7}$CoCrFeNi showed much higher strength due to their fine lamellar microstructure with a large number of *FCC-BCC* interfaces. The 0.7HM homogenized *FCC+BCC*/B2 microstructure showed a quasi-static YS of 830 MPa. However, the ductility is reduced drastically to 20% possibly due to the large volume fraction of hard intermetallic B2 phase. *FCC*-B2 have semi-coherent interfaces, mostly having a Kurdjumov-Sachs (K-S) [22] type orientation relationship (OR) but can also have Nishiyama-Wasserman (N-M) or Pitsch ORs

[23]. The aged 0.7HM-580 condition with *FCC*/$L1_2$+*BCC*/B2 had even higher strength 1076 MPa, almost a 30% increase from 0.7HM, due to precipitate strengthening from $L1_2$ in *FCC* phase which constitutes ~70% volume fraction. The uniform elongation is comparable to 0.7HM condition; the $L1_2$ precipitates did not affect ductility significantly [21].

Strain Rate Sensitivity

During dynamic deformation testing in split-Hopkinson pressure bar, none of the specimens failed at a total test strain of 20%. Flow stresses were distinctly greater in all the four microstructures at high strain rates, 2×10^3 s^{-1}, compared to the quasi-static response. This indicated strong strain rate sensitivity (SRS), a measure of amplification of strength at higher strain rates. The strain rate sensitivity parameter, m, can be calculated from flow stresses at two strain rates as:

$$m = \left[\frac{\partial ln\sigma}{\partial ln\dot{\varepsilon}}\right]_{T,\varepsilon} \qquad (1)$$

where σ is flow stress, ε ̇is strain rate, T is test temperature, and ε is strain. Estimates of SRS parameter m of the four conditions are summarized in Table 1 along with their quasi-static strength and dynamic flow stresses at a very small plastic strain of 0.01.

The strain rate sensitivity of single-phase *FCC* microstructure was exceptionally high at ~0.063. Typically, such large values were only reported in nanocrystalline *FCC* metals [24], [25]. However, HEAs appear to have extraordinary properties in strain rate dependence. Li et al [14] also have reported such a high SRS of 0.053 in a coarse-grained microstructure of single phase *FCC* $Al_{0.3}$CoCrFeNi. Gangireddy et al [12] observed a high SRS of 0.063 in single phase *FCC* $Al_{0.3}$CoCrFeNi and attributed this remarkable property to the significant strength contribution from internal stresses in HEAs, unlike conventional *FCC* metals where they are negligible. In HEAs, large friction stress values were reported due to significant lattice distortion and varying dislocation mobility [15]. Large Peierls-Nabarro (P-N) barriers were reported from Wu et al's observation of severe temperature dependence of tensile properties in CoCrFeMnNi *FCC* HEA [26]. With multiple solute atoms, the HEAs also contain strong solid solution strengthening [27].

Gangireddy et al [13] have also investigated the microstructural dependence of SRS and concluded that the relative contributions from thermal short-range and athermal long-range obstacles to dislocation motion, determine SRS of the yield strength. With slip as the preceding mechanism of deformation before others mechanisms such as twinning or transformation-induced plasticity can initiate, at very small plastic strains before differences in deformation mechanisms can affect strength, yield strength is determined by obstacles to slip alone. The amplitude of long-range obstacles is too large for thermal activation and therefore can be treated as athermal in nature and have no/little dependence on strain rate/temperature. In case of short-range obstacles, where thermal activation can help to overcome such barriers, brings the strain rate dependency.

In simple coarse single phase *FCC* microstructure like 0.3HM, there are only a few long-range obstacles in the form of grain boundaries. As internal stresses make up for majority of YS, an exceptional SRS is demonstrated in this 0.3HM. Even though fine-scale $L1_2$ precipitates

increased strength by 48% in aged 0.3HM-550, they are coherent in nature and thermally activated. So SRS drops only slightly, to m= 0.054, in this *FCC*+$L1_2$ microstructure. The lamellar dual phase microstructures of 0.7HM and 0.7HM-580 both have a high density of interphase boundaries. These long range obstacles do increase strength significantly but being athermal barriers, they also reduce SRS drastically. The homogenized condition 0.7HM has a SRS of m = 0.018. The aged condition 0.7HM-580 has a comparable m = 0.017, despite a 30% increase in YS from $L1_2$ precipitation. So comparing 0.3HM vs 0.3HM-550 and 0.7HM vs. 0.7HM-580 conditions, the effect of coherent nano-scale $L1_2$ precipitates on strain rate sensitivity is similar. In both single phase *FCC* and dual phase *FCC-BCC* microstructures, $L1_2$ precipitation causes a significant rise in YS while maintaining the SRS.

Work Hardening

There was a distinct difference in the quasi-static work hardening behavior of these two types of microstructures. The first derivative of true stress-strain curve ($\theta = d\sigma/d\varepsilon$) is plotted as a function of strain in Figure 5 comparing 0.3HM (single phase *FCC*) vs. 0.7HM (dual phase *FCC+BCC*/B2). Both work hardening plots show four distinct stages of work hardening characteristic of low SFE metals [28-29]. The stages of strain-hardening are stage A - steadily decreasing strain-hardening rate; stage B - constant strain-hardening rate; stage C - decreasing strain-hardening rate and a final stage D – back to almost constant strain-hardening rate [28-29]. The stage B has been often related to the initiation of deformation twinning. Similarly, the stage D is correlated with extensive twin intersections [29]. The decrease of strain-hardening rate in stage C is due to the declining rate of primary twinning. In both 0.3HM (single phase *FCC*) vs. 0.7HM (dual phase *FCC+BCC*/B2) alloys, Stage A is characterized by sharply dropping θ followed by steadying in Stage B. However, the characteristics of Stage B are quite dissimilar.

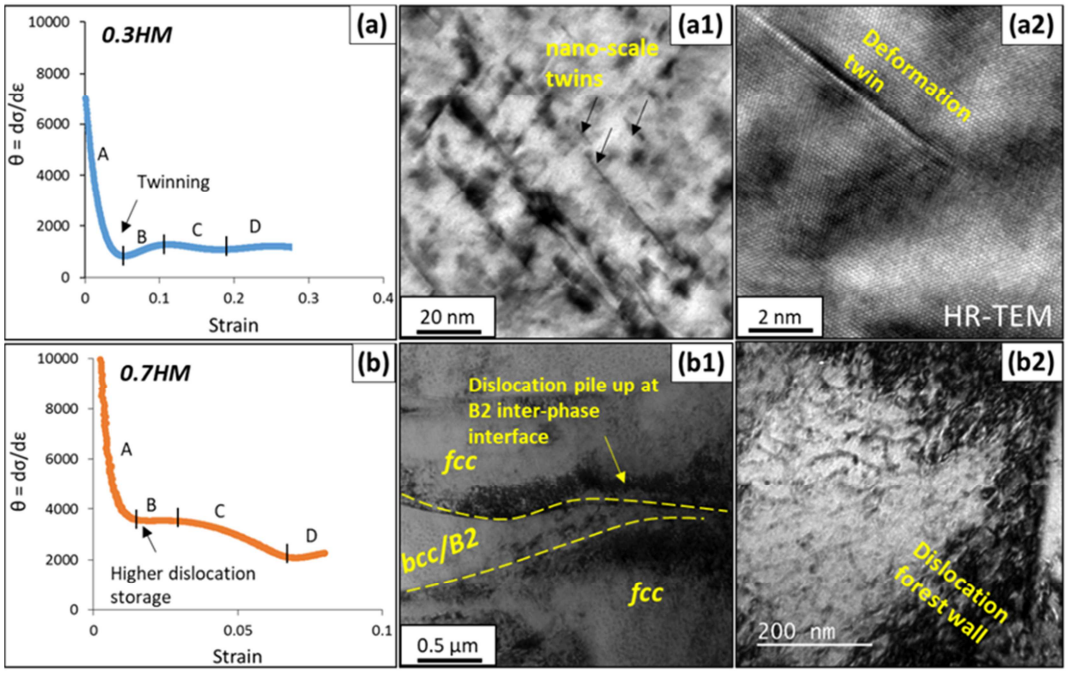

Figure 5: *Comparison of quasi-static work hardening behavior in homogenized single phase and dual phase microstructures. Work hardening-strain plots of (a) 0.3HM, and (b) 0.7HM*

conditions. TEM images of respective post-quasi-static deformation microstructures are on the right. 0.3HM shows a clear upturn in work hardening in stage B indicating twinning and the post-test microstructures (a1) and (a2) show very fine-scale deformation twins. 0.7HM shows a plateau stage B, but at a higher level indicating higher dislocation storage, characteristic in lamellar microstructures with mechanical contrast between phases. The post-quasi-static test microstructures shows (b1) heavy dislocation pileups in the softer FCC phase at the BCC/B2 interphase interface, and (b2) shows some dislocation forests in cell like structure (with dense walls and nearly clean interior) in FCC phase.

In 0.3HM, the work hardening dropped to nearly 1000 MPa at the end of Stage A. After this, it shows a clear upturn in stage B which is usually related to onset of primary twinning [28-29]. TEM images of post-tensile test microstructures indeed showed fine-scale twins Figures 5(a1-a2). Dissociation of several dislocations into 1/6 <112> Shockley partials was reported by Otto et al. [30-Otto] in a single phase *FCC* HEA with low SFE, CoCrFeNiMn. $Al_{0.3}$CoCrFeNi is estimated to have further lower SFE < 30 mJ/mm^2 promoting wider separation between dislocation partials [17]. Inhibition of cross-slip/dislocation climb and suppression of dynamic recovery processes may lead to twinning in this *FCC* structure even at quasi-static strain rates [31].

In 0.7HM, Stage A ended at a much higher θ level = 3200 MPa, after which the stage B appears like a plateau with flat work hardening. This indicates higher dislocation storage, which is typical in fine lamellar structures with mechanical contrast between the phases [32, 33]. The *FCC* phase is generally much softer than the *BCC*/B2 phase in Al_XCoCrFeNi [7-8]. A recent study testing nanopillars from individual phases of $Al_{0.7}$CoCrFeNi showed that the *BCC* phase has roughly 1.8 times the strength of *FCC* phase [34]. *FCC* therefore would deform first leading to strain incompatibilities at interfaces and an inhomogeneous deformation field that in turn translates to building up of internal stresses, which are accommodated by higher storage of geometrically necessary dislocations at interfaces [33]. The interfaces further act as barriers to dislocation motion and pin their movement [11]. The post-test microstructures in Figure 5(b1) showed a heavy pile up of dislocations in the softer *FCC* phase at the *BCC*/B2 interphase interface, while the *BCC*/B2 itself appears relatively defect free. The refined lamellar grain size would elevate twinning stress in 0.7HM and retard twinning [28]. In structures like these where twinning stress is high, other phenomenon like dislocation locking can be dominant [35] and the effect of such barriers is reported to increase with tendency for slip planarity, which would be high here due to low SFE, high P-N stress, and presence of short range ordering (in the case of 0.7HM-580). So despite the absence of deformation twinning, the dual phase microstructure demonstrates higher work hardening in quasi-static regime. The elemental composition of *FCC* phase in 0.7HM is comparable to ~$Al_{0.1}$CoCrFeNi, while the 0.3HM has higher Al content in the *FCC* phase. SFE is expected to decrease with Al addition due to its larger atomic size [14], which leads to prolonged linear hardening stage. Accordingly, we observe that Stage B of 0.3HM sustains for much longer strain than that of 0.7HM [35].

The dynamic work hardening rates of the four conditions are estimated from slope of best linear fit of the true stress-strain curve at high strain rate and presented in Table 1. The dual phase microstructures once again show higher work hardening rates than single phase structures. However, there is a distinct contrast in the effect of precipitates as they are introduced into each of these microstructures.

Table 1. *Summary of quasi-static strength, dynamic flow stress, and strain rate sensitivities of the two microstructures with different grain sizes.*

	Treatment	$\boldsymbol{\sigma(\dot{\varepsilon} = 10^{-3})}$ **(MPa)**	**Dynamic** $\boldsymbol{\sigma(\dot{\varepsilon} = 10^{3})}$ **(MPa)**	**Strain Rate Sensitivity** $\boldsymbol{m = \left[\frac{\partial ln\sigma}{\partial ln\dot{\varepsilon}}\right]_{\varepsilon=0.01}}$	**Dynamic Work Hardening** $\boldsymbol{\theta = \left[\frac{d\sigma}{d\varepsilon}\right]_{\dot{\varepsilon}=10^{3}}}$ **(MPa)**
0.3HM	$Al_{0.3}$CoCrFeNi Homogenized 50%CR + 1150°C/1h	157	390	0.063	1600
0.3HM-550	$Al_{0.3}$CoCrFeNi Aged 50%CR + 1150°C/1h + 550°C/150h	233	525	0.054	2450
0.7HM	$Al_{0.7}$CoCrFeNi Homogenized 30%CR + 1100°C/1h	830	1077	0.018	2100
0.7HM-580	$Al_{0.7}$CoCrFeNi Annealed 30%CR + 1100°C/1h + 580°C/24h	1076	1435	0.017	2050

In the single phase *FCC* microstructure, 0.3HM, the dynamic work hardening was 1600 MPa, which is remarkably high compared to conventional alloys. This is attributed to deformation twining becoming more dominant as cross-slip is further suppressed at higher strain rates. Twin boundaries block propagation of dislocation slip and decrease slip barrier spacing in a dynamic "Hall-Petch" effect [36]. The FCC HEA $Al_{0.3}$CoCrFeNi has been shown to have a very high Hall-Petch coefficient, above 800 MPa/$\mu m^{0.5}$ [21, 37]. So work hardening from deformation twining will be elevated in such a material than conventional FCC alloys. Deformation twin boundaries are also more hardenable than high angle grain boundaries, since twin boundaries lose coherency during plastic flow [38, 39]. Unlike the post-test microstructure after quasi-static testing in Figures 5(a1-a2) which showed nanoscale twins, the post-SHPB microstructures had deformation twins detected even in EBSD, as seen from Figure 6(a). Misorientation profiling along the highlighted lines (Lines 1, 2 in Figure 6(c) below) confirmed the dark lines in the EBSD images to be twin fault planes with their characteristic 60° misorientation. In aged 0.3HM-550 condition with *FCC + $L1_2$*, the precipitates can act as barriers to dislocation motion and their back stresses make them potential twin nucleation sites, enhancing overall twinning activity. This kind of a phenomenon of enhanced work hardening from precipitation is often observed in aged HCP metals [39, 40]. Robson et al reported that nano-scale precipitates increased twin density by 65% in Mg-5%Zn alloy [40]. Strengthening here is based on a shearing mechanism to achieve high cutting forces required for partial dislocations to cut through coherent $L1_2$ precipitates and thus produce plastic deformation [41, 42]. Extensive twinning was observed in the post-SHPB deformed 0.3HM-550, which demonstrated an astounding dynamic

work hardening rate dσ/dε = 2450 MPa. These deformation twins were also detected even at low magnification level as seen from EBSD in Figure 6(b) and misorientation profile along Line 3 in Figure 6(c). A bright-field TEM (BF-TEM) image of twinned region in 0.3HM-550 is depicted in Figure 6(d) demonstrating large-scale deformation twins. The width of these twins varied from couple of nanometers to tens of nanometers.

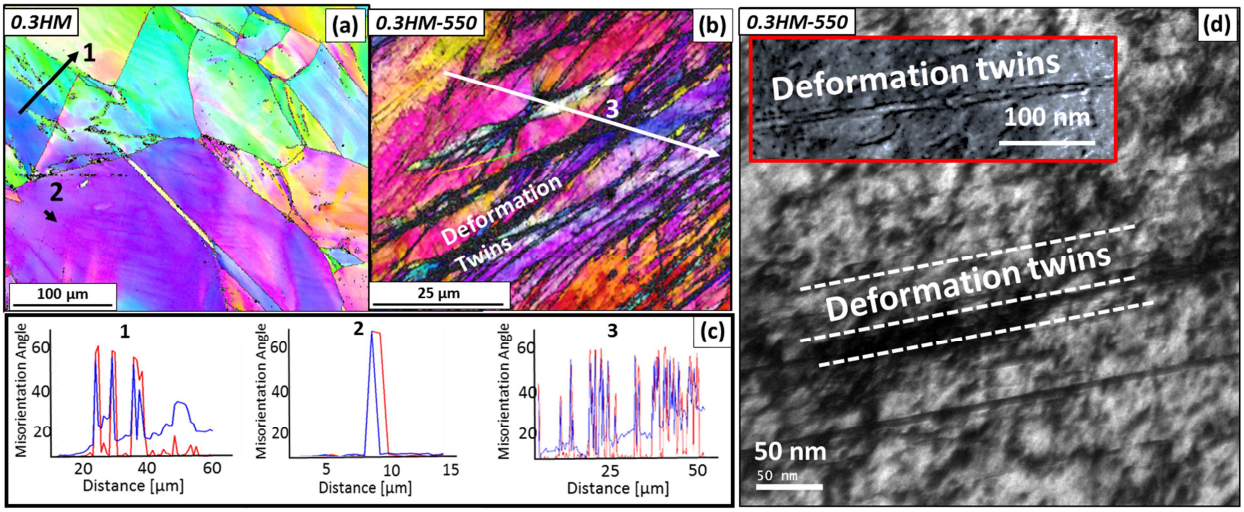

Figure 6. *$Al_{0.3}$CoCrFeNi Microstructures after SHPB deformation at high strain rates: (a) EBSD of 0.3HM homogenized FCC microstructure and (b) 0.3Hm-550 aged FCC+ $L1_2$ microstructure showing large scale deformation twins, (c) misorientation profiling along linear lines confirming the 60° twin fault planes, (d) BF-TEM image of 0.3HM-550 highlighting the deformation twin (inset shows the high magnification image).*

Both the dual phase microstructures, on the other hand, showed dynamic work hardening ~ 2050 MPa. The presence of precipitates did not cause much difference in the θ of aged condition 0.7HM-580. EBSD of post-SHPB microstructures of both 0.7HM and 0.7HM-580 conditions showed only disruption in the lamellar structure, Figures 7(a) and 7(b). It was difficult to characterize deformation twins on SEM examination in $Al_{0.7}$CoCrFeNi alloy. However, at higher magnifications, in TEM, nano-scale twins of 10-20 nm thickness were observed in the *FCC* phase in (1-11) direction in both samples, Figures 7(c) and 7(d). The inset images in Figures 7 (c and d) show the $[011]_{FCC}$ and $[011]_{B2}$ zone axis respectively to confirm the identify of each phase. The BFTEM image from the B2/BCC region in 0.7HM in Figure 7 (c)(right side), shows presence of periodic faults in the structure. Fine lamellar size inhibited the propensity of deformation twinning [28] and limited their growth. The density and scale of twins is lesser than observed in single-phase microstructure (HM0.3) at similar strain level of ε =0.2. Further, the elevated twinning stress levels here appear to be too high for the back stresses from $L1_2$ precipitates to promote twinning in HM0.7-580. Density/thickness of deformation twins in 0.7HM and 0.7HM-580 remain comparable, as do their dynamic work hardening rates.

Figure 7. *$Al_{0.3}$CoCrFeNi microstructures after SHPB deformation at high strain rates: (a) EBSD of 0.7HM homogenized FCC+BCC/B2 microstructure, (b) 0.7HM-580 aged FCC/ $L1_2$ + BCC/B2 conditions both showing disrupted lamellar structure after deformation but no twins were detected at this magnification level. (c) BF-TEM of 0.7HM and (d) 0.7HM-580 showing nano-scale twins of 10-20 nm thickness in FCC phase.*

Conclusions:

Two Al_XCoCrFeNi high entropy alloys, one of lower Al content x=0.3 with single phase *FCC* structure and another of higher Al content x=0.7 with dual phase *FCC+BCC* near-eutectic structure were chosen. Quasi-static and dynamic mechanical behaviors of these two structures (coarse grained single phase vs fine lamellar dual phase) are compared and contrasted. These precipitation hardenable alloys were also aged to induce ordered intermetallic formation in *FCC* phase and the effect of precipitates was explored. The main findings of this investigation are:

Single vs. Dual phase structure:

- Single phase *FCC* shows low YS of 160 MPa and high ductility of 64%. Dual phase *FCC+BCC* offered much higher YS = 830 MPa due to the numerous interphase boundaries in this near-eutectic lamellar structure while retaining ample ductility ~ 20%.
- The single phase *FCC* coarse alloy showed extraordinary strain rate sensitivity (SRS), m = 0.063. The dynamic flow stresses were significantly higher than their quasi-static counterparts. In the dual phase alloy, the athermal nature of the *FCC-BCC* interphase boundaries lowered SRS to m = 0.018.
- Strong work hardening in the coarse *FCC* alloy arose from deformation twinning. The twins were nanoscale in width after quasi-static deformation but were thicker after dynamic deformation. The dual phase alloy showed even higher quasi-static work hardening due to its higher dislocation storage capacity. The lamellar structures exhibited no twinning after quasi-static deformation but displayed nano-scale twins after dynamic deformation. Twinning was suppressed due to the refined lamellae width (2-3um) compared to the coarse single phase *FCC* grains of 150 um diameter. Reduction in *FCC* grain size elevated twinning stress and retarded twin nucleation.

Effect of coherent precipitates:

- Coherent nano-scale $L1_2$ precipitate boundaries are thermal obstacles. Introduction of a large density of $L1_2$ into the *FCC* phase resulted in significant YS spike in both types of microstructures, 48% in *FCC* and 30% in *FCC+BCC.* But they did not reduce SRS.
- Introduction of $L1_2$ into single phase *FCC* caused a massive surge in deformation twin density. Twin nucleation stress is low in this low SFE, coarse structure and appears to have been overcome easily by the back stresses at the precipitates enhancing twinning activity. The dynamic work hardening hence showed a spike to 2400 MPa. In contrast, presence of $L1_2$ in *FCC* phase of the dual phase microstructure did not cause much difference. The twinning activity remained more or less similar. Twinning stress in the fine *FCC* lamellae appears to be too high for the back stresses from the precipitates to trigger further twin nucleation.

Acknowledgment:

The work was performed under a cooperative agreement between the Army Research Laboratory and the University of North Texas (W911NF-16-2-0189). We also acknowledge the Materials Research Facility at the University of North Texas for microscopy facilities.

References:

1. Jien-Wei, Y. (2006). Recent progress in high entropy alloys. Ann. Chim. Sci. Mat, 31(6), 633-648.
2. Yeh, Jien-Wei, Swe-Kai Chen, and Yu-Liang Chen. "Novel alloy concept, challenges and opportunities of high-entropy alloys." In Frontiers in the design of materials, pp. 31-47. CRC Press, 2007.
3. Gwalani, B., Gorsse, S., Choudhuri, D., Styles, M., Zheng, Y., Mishra, R. S., & Banerjee, R. Modifying transformation pathways in high entropy alloys or complex concentrated alloys via thermo-mechanical processing. Acta Materialia 153, (2018) 169-185.
4. Zhang, Yong, Yun Jun Zhou, Jun Pin Lin, Guo Liang Chen, and Peter K. Liaw. "Solid-solution phase formation rules for multi-component alloys." Advanced Engineering Materials 10, no. 6 (2008): 534-538..
5. Gao, Michael C., Jien-Wei Yeh, Peter K. Liaw, and Yong Zhang. High-Entropy Alloys. Springer International Publishing, 2016.
6. Tsai, Ming-Hung, and Jien-Wei Yeh. "High-entropy alloys: a critical review." *Materials Research Letters* 2, no. 3 (2014): 107-123.
7. Wang, Woei-Ren, Wei-Lin Wang, and Jien-Wei Yeh. "Phases, microstructure and mechanical properties of AlxCoCrFeNi high-entropy alloys at elevated temperatures." Journal of Alloys and Compounds 589 (2014): 143-152.
8. Wang, Woei-Ren, Wei-Lin Wang, Shang-Chih Wang, Yi-Chia Tsai, Chun-Hui Lai, and Jien-Wei Yeh. "Effects of Al addition on the microstructure and mechanical property of AlxCoCrFeNi high-entropy alloys." *Intermetallics* 26 (2012): 44-51.
9. Joseph, Jithin, Nicole Stanford, Peter Hodgson, and Daniel Mark Fabijanic. "Understanding the mechanical behaviour and the large strength/ductility differences between *FCC* and *BCC* AlxCoCrFeNi high entropy alloys." *Journal of Alloys and Compounds* 726 (2017): 885-895.
10. Lu, Yiping, Yong Dong, Sheng Guo, Li Jiang, Huijun Kang, Tongmin Wang, Bin Wen et al. "A promising new class of high-temperature alloys: eutectic high-entropy alloys." *Scientific reports* 4 (2014): 6200.
11. Crouch, Ian, ed. *The science of armour materials*. Woodhead Publishing, 2016.
12. Gangireddy, Sindhura, Bharat Gwalani, Kaimiao Liu, Rajarshi Banerjee, and Rajiv S. Mishra. "Microstructures with extraordinary dynamic work hardening and strain rate sensitivity in Al0. 3CoCrFeNi high entropy alloy." Materials Science and Engineering: A 734 (2018): 42-50.

13. Gangireddy, Sindhura, Liu Kaimiao, Bharat Gwalani, and Rajiv Mishra. "Microstructural dependence of strain rate sensitivity in thermomechanically processed Al0. 1CoCrFeNi high entropy alloy." *Materials Science and Engineering: A* 727 (2018): 148-159.
14. Li, Z., S. Zhao, H. Diao, P. K. Liaw, and M. A. Meyers. "High-velocity deformation of Al 0. 3 CoCrFeNi high-entropy alloy: Remarkable resistance to shear failure." *Scientific Reports* 7 (2017): 42742.
15. Kumar, N., M. Komarasamy, P. Nelaturu, Z. Tang, P. K. Liaw, and R. S. Mishra. "Friction stir processing of a high entropy alloy Al 0.1 CoCrFeNi." *Jom* 67, no. 5 (2015): 1007-1013.
16. Zhang, Y., X. Yang, and P. K. Liaw. "Alloy design and properties optimization of high-entropy alloys." *Jom* 64, no. 7 (2012): 830-838.
17. Kumar, N., Q. Ying, X. Nie, R. S. Mishra, Z. Tang, P. K. Liaw, R. E. Brennan, K. J. Doherty, and K. C. Cho. "High strain-rate compressive deformation behavior of the Al0. 1CrFeCoNi high entropy alloy." *Materials & Design* 86 (2015): 598-602.
18. Chen, Weinong W., and Bo Song. *Split Hopkinson (Kolsky) bar: design, testing and applications*. Springer Science & Business Media, 2010.
19. Liu, Gang, Lin Liu, Xinwang Liu, Zhijun Wang, Zhenhua Han, Guojun Zhang, and A. Kostka. "Microstructure and mechanical properties of Al 0.7 CoCrFeNi high-entropy-alloy prepared by directional solidification." *Intermetallics* 93 (2018): 93-100.
20. Tong, Chung-Jin, Yu-Liang Chen, Jien-Wei Yeh, Su-Jien Lin, Swe-Kai Chen, Tao-Tsung Shun, Chun-Huei Tsau, and Shou-Yi Chang. "Microstructure characterization of AlxCoCrCuFeNi high-entropy alloy system with multiprincipal elements." *Metallurgical and Materials Transactions A* 36, no. 4 (2005): 881-893.
21. Gwalani, B., Vishal Soni, Michael Lee, S. A. Mantri, Yang Ren, and R. Banerjee. "Optimizing the coupled effects of Hall-Petch and precipitation strengthening in a Al0. 3CoCrFeNi high entropy alloy." *Materials & Design* 121 (2017): 254-260.
22. Gwalani, B., V. Soni, D. Choudhuri, M. Lee, J. Y. Hwang, S. J. Nam, H. Ryu, Soon Hyung Hong, and R. Banerjee. "Stability of ordered L12 and B2 precipitates in face centered cubic based high entropy alloys-Al0. 3CoFeCrNi and Al0. 3CuFeCrNi2." *Scripta Materialia* 123 (2016): 130-134.
23. Choudhuri, Deep, Shivakant Shukla, Whitley B. Green, Bharat Gwalani, Victor Ageh, Rajarshi Banerjee, and Rajiv S. Mishra. "Crystallographically degenerate B2 precipitation in a plastically deformed *FCC*-based complex concentrated alloy." *Materials Research Letters* 6, no. 3 (2018): 171-177.
24. Valiev, R. Z., I. V. Alexandrov, Y. T. Zhu, and T. C. Lowe. "Paradox of strength and ductility in metals processed bysevere plastic deformation." *Journal of Materials Research*17, no. 1 (2002): 5-8.
25. Wei, Q., S. Cheng, K. T. Ramesh, and E. Ma. "Effect of nanocrystalline and ultrafine grain sizes on the strain rate sensitivity and activation volume: *FCC* versus *BCC* metals." *Materials Science and Engineering: A* 381, no. 1-2 (2004): 71-79.

26. Wu, Zhenggang, Hongbin Bei, George M. Pharr, and Easo P. George. "Temperature dependence of the mechanical properties of equiatomic solid solution alloys with face-centered cubic crystal structures." *Acta Materialia* 81 (2014): 428-441.
27. Zhang, Y., X. Yang, and P. K. Liaw. "Alloy design and properties optimization of high-entropy alloys." *Jom* 64, no. 7 (2012): 830-838.
28. El-Danaf, Ehab, Surya R. Kalidindi, and Roger D. Doherty. "Influence of grain size and stacking-fault energy on deformation twinning in *FCC* metals." *Metallurgical and Materials Transactions A* 30, no. 5 (1999): 1223-1233.
29. Asgari, Sirous, Ehab El-Danaf, Surya R. Kalidindi, and Roger D. Doherty. "Strain hardening regimes and microstructural evolution during large strain compression of low stacking fault energy *FCC* alloys that form deformation twins." *Metallurgical and Materials Transactions A* 28, no. 9 (1997): 1781-1795.
30. Otto, Frederik, A. Dlouhý, Ch Somsen, Hongbin Bei, G. Eggeler, and Easo P. George. "The influences of temperature and microstructure on the tensile properties of a CoCrFeMnNi high-entropy alloy." *Acta Materialia* 61, no. 15 (2013): 5743-5755.
31. Gray III, George T. "High-strain-rate deformation: mechanical behavior and deformation substructures induced." *Annual Review of Materials Research* 42 (2012): 285-303.
32. Bartholomeusz, Michael F., Mark A. Cantrell, and John A. Wert. "The enhanced work hardening rates of the constituent TiAl and Ti3Al phases in a lamellar microstructure." *Materials Science and Engineering: A* 201, no. 1-2 (1995): 24-31.
33. de Formanoir, Charlotte, Alice Brulard, Solange Vivès, Guilhem Martin, Frédéric Prima, Sébastien Michotte, Edouard Rivière, Adrien Dolimont, and Stéphane Godet. "A strategy to improve the work-hardening behavior of Ti–6Al–4V parts produced by additive manufacturing." *Materials Research Letters* 5, no. 3 (2017): 201-208.
34. Giwa, Adenike M., Peter K. Liaw, Karin A. Dahmen, and Julia R. Greer. "Microstructure and small-scale size effects in plasticity of individual phases of Al 0.7 CoCrFeNi High Entropy alloy." *Extreme Mechanics Letters* 8 (2016): 220-228.
35. Hamdi, Farzad, and Sirous Asgari. "Evaluation of the role of deformation twinning in work hardening behavior of face-centered-cubic polycrystals." *Metallurgical and Materials Transactions A* 39, no. 2 (2008): 294-303.
36. Rohatgi, Aashish, Kenneth S. Vecchio, and George T. Gray. "The influence of stacking fault energy on the mechanical behavior of Cu and Cu-Al alloys: deformation twinning, work hardening, and dynamic recovery." *Metallurgical and Materials Transactions A* 32, no. 1 (2001): 135-145.
37. Gangireddy, S., Gwalani, B. and Mishra, R.S., "Grain Size Dependence of Strain Rate Sensitivity in a Single Phase FCC High Entropy Alloy Al0. 3CoCrFeNi." *Materials Science and Engineering: A 736* (2018): 344-348.
38. Cao, A. J., and Y. G. Wei. "Molecular dynamics simulation of plastic deformation of nanotwinned copper." *Journal of Applied Physics* 102, no. 8 (2007): 083511.

39. Ma, E., Y. M. Wang, Q. H. Lu, M. L. Sui, L. Lu, and K. Lu. "Strain hardening and large tensile elongation in ultrahigh-strength nano-twinned copper." *Applied physics letters* 85, no. 21 (2004): 4932-4934.
40. Robson, J. D., N. Stanford, and M. R. Barnett. "Effect of particles in promoting twin nucleation in a Mg–5 wt.% Zn alloy." *Scripta materialia* 63, no. 8 (2010): 823-826.
41. Gao, Xiangyu, Rui Hu, and Jieren Yang. "The effect of Ni 3 (Cr 0.2 W 0.4 Ti 0.4) particles with DO 22 structure on the deformation mode and mechanical properties of the aged Ni-Cr-W-Ti alloy." *Scripta Materialia* 153 (2018): 44-48.
42. Gutierrez-Urrutia, I., and D. Raabe. "Influence of Al content and precipitation state on the mechanical behavior of austenitic high-Mn low-density steels." *Scripta Materialia* 68, no. 6 (2013): 343-347.